

Loss of cell division cycle-associated 5 promotes cell apoptosis by activating DNA damage response in clear cell renal cell carcinoma

XING HUANG^{1*}, YAN HUANG^{1*}, ZHENG LV², TAO WANG¹, HUAYI FENG¹,
HANFENG WANG¹, SONGLIANG DU¹, SHENGPAN WU¹, DONGLAI SHEN¹,
CHENFENG WANG¹, HONGZHAO LI¹, BAOJUN WANG¹, XIN MA¹ and XU ZHANG¹

¹Department of Urology, The Third Medical Center, Chinese PLA General Hospital/Medical School of Chinese PLA/State Key Laboratory of Kidney Diseases, Chinese PLA General Hospital, Beijing 100853;

²Department of Urology, The Third Affiliated Central Hospital of Nankai University, Tianjin 300071, P.R. China

Received March 17, 2022; Accepted May 18, 2022

DOI: 10.3892/ijo.2022.5377

Abstract. Cell division cycle-associated 5 (CDCA5) protein, which is involved in cohesion, contributes to cell cycle regulation and chromosome segregation by maintaining genomic stability. Accumulating evidence indicates that CDCA5 expression is upregulated in a number of types of cancer associated with a poor prognosis. However, the biological function of CDCA5 in clear cell renal cell carcinoma (ccRCC) remains largely unknown. In the present study, The Cancer Genome Atlas data mining revealed that CDCA5 was more highly expressed in ccRCC than in adjacent normal tissues. Importantly, such a high expression was associated with a higher risk of distant metastasis and poorer clinical outcomes. Moreover, the clinical and prognostic value of CDCA5 expression was further investigated using immunohistochemistry on tissue microarrays containing paired tumor tissues and adjacent normal tissues from 137 patients with ccRCC. Functional analyses revealed that CDCA5 knockdown significantly inhibited the proliferation and migration of ccRCC cells, and suppressed the growth of xenografts in nude mice. Mechanistically, CDCA5 knockdown induced severe DNA

damage with the persistent accumulation of γ -H2A histone family member X foci, resulting in G2/M cell cycle arrest and finally, in chromosomal instability and apoptosis. CDCA5 knockdown significantly decreased the phosphorylation levels of Stat3 and NF- κ B, suggesting that CDCA5 plays a role in regulating the inflammatory response. Collectively, the findings of the present study indicate that ccRCC cells require CDCA5 for malignant progression, and that CDCA5 inhibition may enhance the outcomes of patients with high-risk ccRCC.

Introduction

Kidney cancer is currently the 11th leading malignancy incidence among males (254,507 cases) and the 16th common among females (148,755 cases), ranking as the 14th most common cause of cancer-associated mortality (175,098 cases) worldwide in 2018 (1). Based on intratumor heterogeneity and biological characteristics (2,3), genetic diversity determines varying responses to therapy, and can even lead to drug resistance by some key determinants, including imposing therapeutic pressures (4). Thus, it is of utmost urgency to identify a novel therapeutic target. Moreover, apart from the WHO/ISUP grade which is widely used to evaluate tumor malignancy, effective biomarkers are less exploited for the profiling of renal cell carcinoma (RCC).

Cell division cycle-associated 5 (CDCA5), also known as sororin, is a substrate of APC/CCdc20 (anaphase-promoting complex/cyclosome associated with Cdc20) (5), playing pivotal roles in sister chromatid cohesion (6), chromatin structure (7), genome integrity (8) and DNA damage repair (9,10). Cohesin is a 'ring structure' complex composed of certain core subunits, such as structural maintenance of chromosomes protein (SMC)1, SMC3, RAD21 and stromal antigen 1/2 (11). CDCA5 antagonizes Wings apart-like protein homolog (WAPL) to adjust the loading and unloading of cohesin, thus stabilizing cohesin-DNA interactions in the S and G2/M phases (12).

Recent studies have discovered that the upregulated expression of CDCA5 is associated with an increased tumor malignancy as an indicator of an unfavorable prognosis, including in hepatocellular carcinoma (13), colorectal cancer (14), urothelial carcinoma (15), etc. However, several

Correspondence to: Professor Xu Zhang or Professor Xin Ma, Department of Urology, The Third Medical Center, Chinese PLA General Hospital/Medical School of Chinese PLA/State Key Laboratory of Kidney Diseases, Chinese PLA General Hospital, 28 Fuxing Road, Haidian, Beijing 100853, P.R. China
E-mail: xzhang301@163.com
E-mail: urologist@foxmail.com

*Contributed equally

Abbreviations: ccRCC, clear cell renal cell carcinoma; CDCA5, cell division cycle-associated 5; TMA, tissue microarray; DFS, disease-free survival; OS, overall survival; DDR, DNA damage response; shRNA, short hairpin RNA; RT-qPCR, reverse-transcription quantitative polymerase chain reaction

Key words: cell division cycle-associated 5, DNA damage, apoptosis, ccRCC, prognostic factor

underlying processes of CDCA5 involved in coordinated chromatin remodeling and tumorigenesis are not yet well characterized. When paired with advanced pathological stages and tumor grade, the expression of CDCA5 lacks a significant association in the majority of these tumors to effectively stratify tumor malignancy. Additionally, CDCA5 is not as effective at predicting survival outcomes in these cancer types, as it is in clear cell RCC (ccRCC). In addition, to the best of our knowledge, there has been no report to date describing the expression and function of CDCA5 in RCC.

The objective of the present study was to investigate the prognostic value of CDCA5 expression levels in ccRCC and to shed light on tumorigenesis associated with CDCA5. In this regard, for the first time, to the best of our knowledge, the present study delineated the differences in CDCA5 expression between ccRCC tumor specimens and adjacent normal tissues. Of note, the more advanced grades and stages of ccRCC exhibited a higher expression of CDCA5, predicting an unfavorable survival. *In vivo* and *in vitro* experiments were conducted to investigate the function and underlying mechanisms of CDCA5 in the malignant progression of ccRCC. Apart from the previously described roles in cell proliferation, chromatin cohesion maintenance and cell cycle regulation (12,16), it was demonstrated that CDCA5 could function via the DNA damage response (DDR) pathway in ccRCC and trigger sequential cell cycle arrest and apoptosis when its expression was knocked down.

The findings presented herein support the oncogenic role of CDCA5 in maintaining genomic stability and promoting inflammatory signals, thus promoting ccRCC survival and progression. CDCA5 may thus be a novel biomarker and potential therapeutic target in ccRCC.

Materials and methods

Data mining. To identify differential expressed genes (DEGs), The Cancer Genome Atlas (TCGA) dataset (<http://genome-cancer.ucsc.edu>) was used to screen all genes positively associated with a poor prognosis of RCC. Gene Ontology and Kyoto Encyclopedia of Genes and Genomes (KEGG) pathway enrichment analysis revealed that the majority of these DEGs were associated with cell cycle control. Following the tumor survival analysis of these hub genes, it was found that CDCA5 was overexpressed in ccRCC and predicted a poor patient prognosis (Figs. 1 and 2). Subsequently, Gene Set Cancer Analysis (GSCA, <http://bioinfo.life.hust.edu.cn/GSCA/#/expression>) and the UALCAN database (<http://ualcan.path.uab.edu/index.html>) was utilized to analyze the differential expression patterns of CDCA5 in all the 33 TCGA cancers. Thereafter, based on the CDCA5 expression differences between tumor and normal samples, GSCA was used to evaluate the association between the Gene Set Variation Analysis (GSVA) score and patient survival.

Patients and tumor specimens. From October, 2012 to May, 2016, a total of 137 patients who underwent RCC resection at Chinese People's Liberation Army (PLA) General Hospital (Beijing, China) were enrolled in the present study. Resected paired tumor and adjacent normal tissue were immediately snap-frozen in liquid nitrogen, and then stored at -80°C .

Written informed consent was obtained from all participants. The study was conducted in accordance with protocol approved by the Protection of Human Subjects Committee of Chinese People's Liberation Army (PLA) General Hospital (S2019-219-07). The clinicopathological characteristics of these patients with ccRCC are summarized in Table I. The TNM classification (American Joint Committee on Cancer eighth edition) was utilized for staging ccRCC (17). The inclusion criteria were as follows: Conventional surgical treatment without radiation or chemotherapy, histopathologically diagnosed ccRCC, post-operative follow-up for at least 12 months and comprehensive clinical medical records. Patients with severe underlying conditions, patients with inadequate data and patients with benign renal tumors, Xp11.2 translocation/TFE3 fusion gene-related renal carcinoma, papillary carcinoma and other non-clear cell carcinomas were excluded from the study.

Cell lines and cell culture. The RCC cell lines, ACHN (PUMC000334), Caki-1 (PUMC000244), A498 (PUMC000171), OSRC2 (PUMC000292), 769-P (PUMC000333) and 786-O (PUMC000243), and 293T (PUMC000010) cells were purchased from the National Infrastructure of Cell Line Resource (Beijing, China). SN12-PM6 cell line was kindly provided by Dr X.P. Zhang from Union Hospital, Tongji Medical College, Huazhong University of Science and Technology, Wuhan, China. The 293T and SN12-PM6 cell lines were cultured in Dulbecco's modified Eagle's medium; the ACHN and A498 cells were maintained in minimum essential medium; the OSRC2, 769-P and 786-O cells were maintained in Roswell Park Memorial Institute-1640 medium; and the Caki-1 cells were maintained in McCoy's 5A medium. All media (Thermo Fisher Scientific, Inc.) were supplemented with 10% fetal bovine serum (FBS) (EVERY GREEN, Zhejiang Tianhang Biotechnology Co., Ltd.) and 1% penicillin G sodium/streptomycin. And all cell lines were grown in a humidified 37°C incubator containing 5% CO_2 .

Plasmid construction and transfection. Short hairpin RNA (shRNA) targeting human CDCA5 was designed and cloned into the lentivirus expression vector, pLKO.1 (Addgene Plasmid 8453). shRNA scramble (Addgene Plasmid 162011) was used as the lentiviral negative control vector. The target sequences for CDCA5 were designed as follows: shCDCA5-1 (forward, 5'-CCGGCCAAAGTACCATAGCCAGTTTCTCGAGAACTGGCTATGGTACTTTGGTTTTG-3' and reverse, 5'-AATTCAAAAACCAAAGTACCA TAGCCAGTTTCTCGAGAACTGGCTATGGTACTTTG G-3') and shCDCA5-2 (forward, 5'-CCGGGAGCAGTTTGA TCTCCTGGTTCTCGAGAACCAGGAGATCAAAGTCTCTTTTG-3' and reverse, 5'-AATTCAAAAAGAGCAGTT TGATCTCCTGGTTCTCGAGAACCAGGAGATCAAAGTCTCTCT-3'). All the recombinant plasmids were verified by DNA sequencing. For recombinant lentivirus production, 293T packaging cells were transfected by using the calcium phosphate reagent (CTK001, Macgene, China) according to manufacturer's instructions with 6 μg packaging DNA, 4.5 μg packaging plasmid (pSPAX2, Addgene Plasmid 12260), and 1.5 μg envelope expressing plasmid (VSV-G/pMD2.G, Addgene Plasmid 12259). Following transfection for 6 h, the

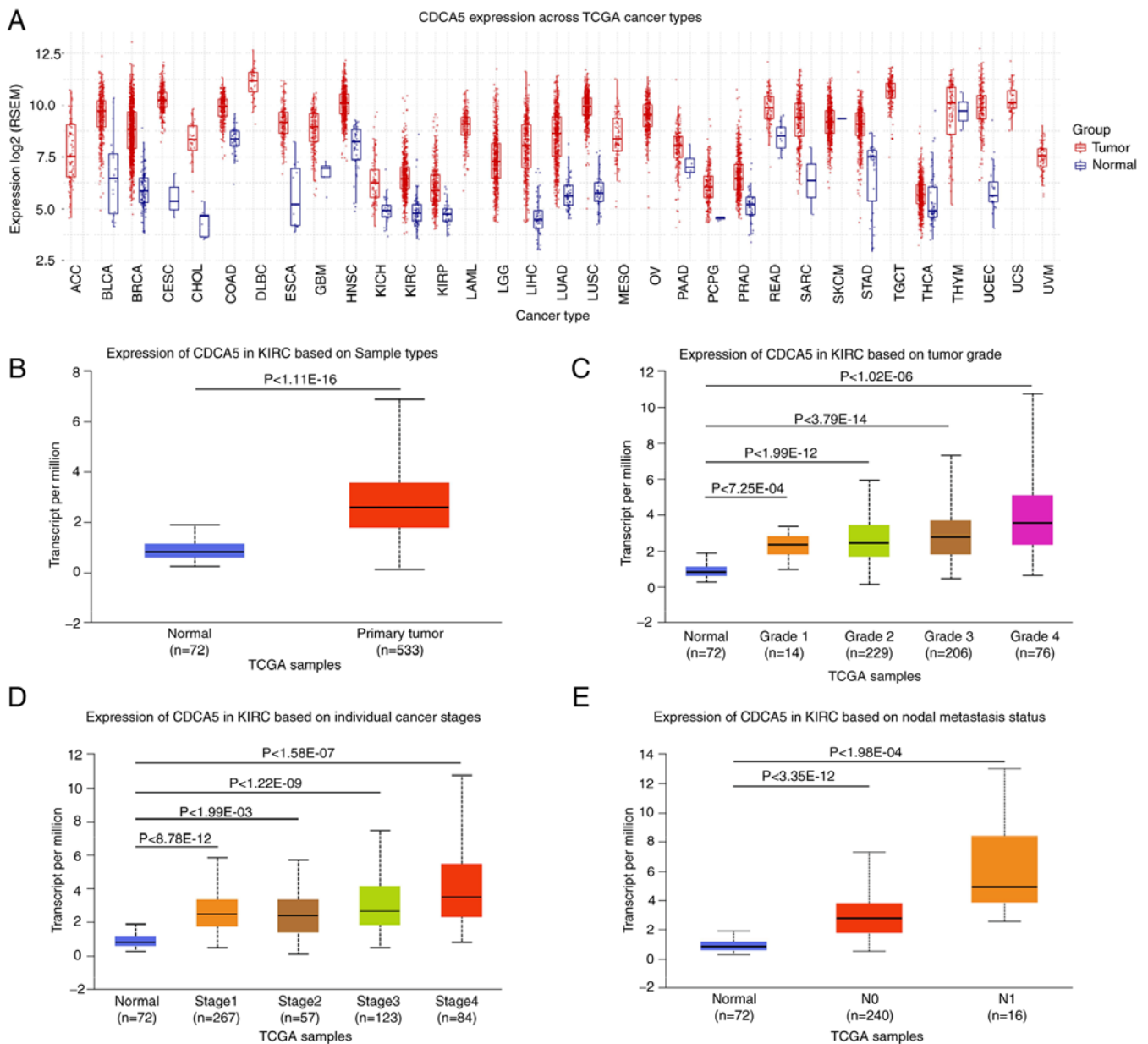


Figure 1. TCGA analysis of kidney renal clear cell carcinoma on UALCA and GSCA. (A) Pancancer relative expression of CDCA5 across 33 TCGA tumors. (B) Differential expression of CDCA5 in ccRCC tissue vs. adjacent normal tissue. (C) Expression of CDCA5 in ccRCC of different tumor grade. (D) Expression of CDCA5 in ccRCC based on nodal metastasis status. (E) Expression of CDCA5 in ccRCC based on individual cancer stages. TCGA, The Cancer Genome Atlas; UALCA, the university of Alabama at Birmingham cancer data analysis; GSCA, Gene Set Cancer Analysis; CDCA5, cell division cycle-associated 5; ccRCC, clear cell renal cell carcinoma; ACC, adrenocortical carcinoma; BLCA, bladder urothelial carcinoma; BRCA, breast invasive carcinoma; CESC, cervical squamous cell carcinoma and endocervical adenocarcinoma; CHOL, cholangiocarcinoma; COAD, colon adenocarcinoma; DLBC, lymphoid neoplasm diffuse large B-cell lymphoma; ESCA, esophageal carcinoma; GBM, glioblastoma multiforme; HNSC, head and neck squamous cell carcinoma; KICH, kidney chromophobe; KIRC, kidney renal clear cell carcinoma; KIRP, kidney renal papillary cell carcinoma; LAML, acute myeloid leukemia; LGG, brain lower grade glioma; LIHC, liver hepatocellular carcinoma; LUAD, lung adenocarcinoma; LUSC, lung squamous cell carcinoma; MESO, mesothelioma; OV, ovarian serous cystadenocarcinoma; PAAD, pancreatic adenocarcinoma; PCPG, pheochromocytoma and paraganglioma; PRAD, prostate adenocarcinoma; READ, rectum adenocarcinoma; SARC, sarcoma; SKCM, skin cutaneous melanoma; STAD, stomach adenocarcinoma; TGCT, testicular germ cell tumor; THCA, thyroid carcinoma; THYM, thymoma; UCEC, uterine corpus endometrial carcinoma; UCS, uterine carcinosarcoma; UVM, uveal melanoma.

293T cells were replaced with fresh media. The supernatant was then collected after 48 h, cleared cellular debris by centrifugation at 300 x g for 5 min, and filtered through a 0.45- μ m filter (SLHV033RB, Merck Millipore). The filtered supernatant was collected and added lentivirus precipitation solution (C103, Genstar) to precipitate the virus overnight at 4°C. The viral supernatant was then harvested by centrifugation at 10,000 x g for 20 min at 4°C. The SN12-PM6 and

786O cells were selected for infection with CDCA5 shRNA lentivirus at an optimal multiplicity of infection (MOI) of 10. After infection for 24 h with lentivirus and 10 μ g/ml polybrene in a 37°C incubator, the viral particles were replaced with fresh medium and cells in which CDCA5 was knocked down were selected in the presence of 2 μ g/ml of puromycin for at least 2 days. Western blot analysis and RT-qPCR were conducted to determine the transfection efficiency.

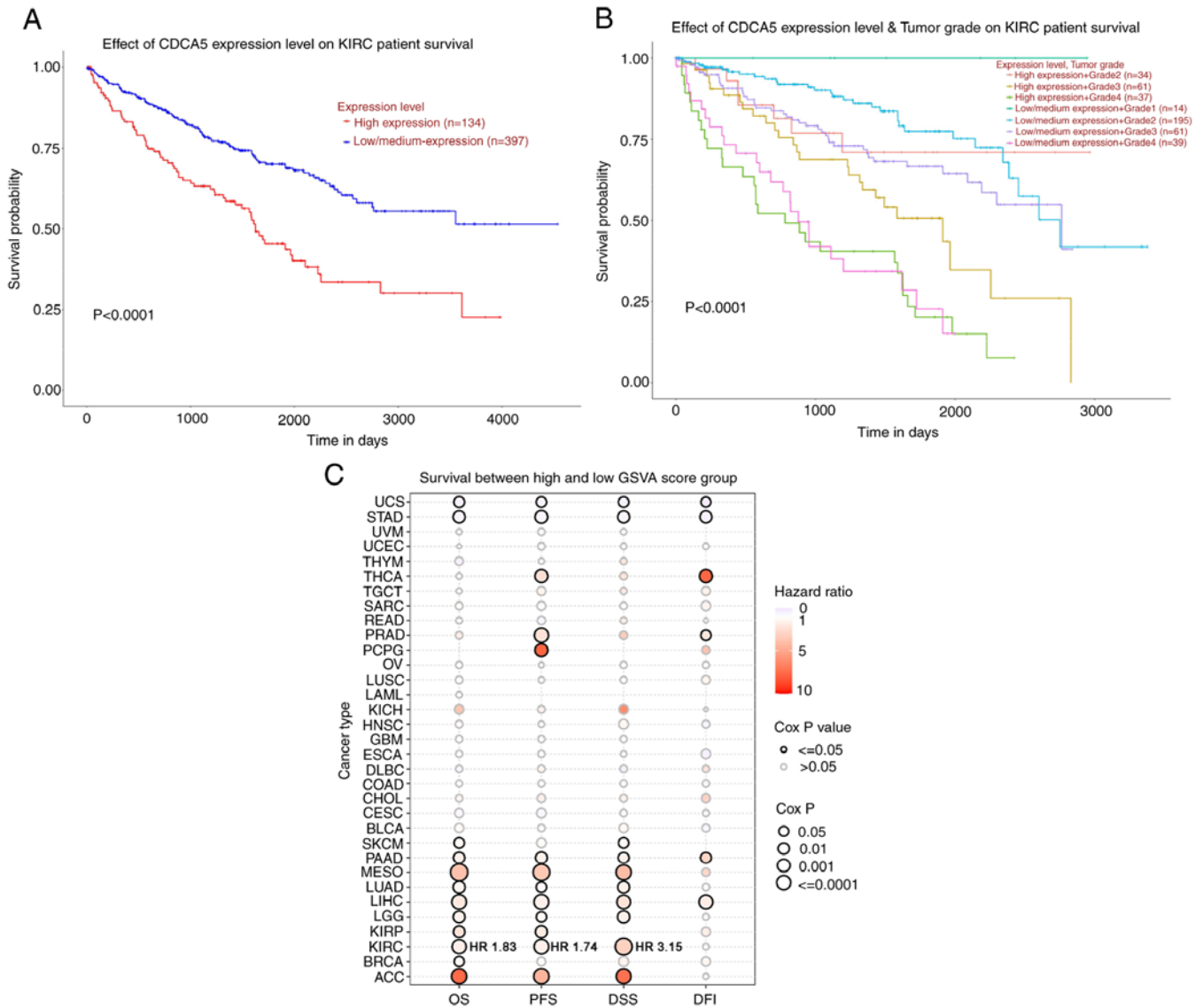


Figure 2. Survival analysis of CDCA5 in kidney renal clear cell carcinoma and TCGA cancers was performed using UALCA and GSEA. (A) Patients with a higher CDCA5 expression exhibited a worse overall survival ($P < 0.0001$) compared to those with a low/medium CDCA5 expression group. (B) Kaplan-Meier curves of overall survival between groups according to CDCA5 expression level and tumor grade. Patients with a high CDCA5 expression and grade 4 ccRCC tumor had a worse survival ($P < 0.0001$). (C) Bubble plot displaying survival between the high and low gene set variation analysis score related to CDCA5 expression. The red bubbles represented a higher hazard ratio, and bubbles with a black outline border indicate a Cox P-value < 0.05 . UALCA, the university of Alabama at Birmingham cancer data analysis; GSEA, Gene Set Cancer Analysis; CDCA5, cell division cycle-associated 5; ccRCC, clear cell renal cell carcinoma; OS, overall survival; DFS, disease-free survival; PFS, progression-free survival; DSS, disease-free survival; DFI, disease-free interval; ACC, adrenocortical carcinoma; BLCA, bladder urothelial carcinoma; BRCA, breast invasive carcinoma; CESC, cervical squamous cell carcinoma and endocervical adenocarcinoma; CHOL, cholangiocarcinoma; COAD, colon adenocarcinoma; DLBC, lymphoid neoplasm diffuse large B-cell lymphoma; ESCA, esophageal carcinoma; GBM, glioblastoma multiforme; HNSC, head and neck squamous cell carcinoma; KICH, kidney chromophobe; KIRC, kidney renal clear cell carcinoma; KIRP, kidney renal papillary cell carcinoma; LAML, acute myeloid leukemia; LGG, brain lower grade glioma; LIHC, liver hepatocellular carcinoma; LUAD, lung adenocarcinoma; LUSC, lung squamous cell carcinoma; MESO, mesothelioma; OV, ovarian serous cystadenocarcinoma; PAAD, pancreatic adenocarcinoma; PCPG, pheochromocytoma and paraganglioma; PRAD, prostate adenocarcinoma; READ, rectum adenocarcinoma; SARC, sarcoma; SKCM, skin cutaneous melanoma; STAD, stomach adenocarcinoma; TGCT, testicular germ cell tumor; THCA, thyroid carcinoma; THYM, thymoma; UCEC, uterine corpus endometrial carcinoma; UCS, uterine carcinosarcoma; UVM, uveal melanoma.

Cell proliferation assay. Cell proliferation assay was performed using crystal violet assay for determining cell viability. The 786-O and SN12-PM6 cells were seeded separately in a six-well plate. Following transfection with lentivirus for 24 h and followed by puromycin selection for 48 h, the cells were fixed with 4% paraformaldehyde for 20 min and stained with 0.1% crystal violet (C0121, Beyotime Institute of Biotechnology) for 20 min at room temperature. The cells were then gently washed with water, and the dye was then

dissolved into acetic acid. The optical density of the collecting solution was measured at 570 nm (OD570) using a plate reader (ELx800, BioTek Instruments, Inc.). The mean value of three independent experiments was calculated.

Cell migration assay. In the cell migration assay, the Boyden chamber was used for 24-well plates. The inserts were coated with polycarbonate Transwell membrane (Corning, Inc.) with an 8- μ m pore size. After refilling with a 500 μ l high

Table I. Association between CDCA5 expression and the clinical characteristics of 137 patients with ccRCC.

Characteristic	No. of patients (%)	CDCA5 expression		χ^2 value	P-value
		Low (%)	High (%)		
Number of patients	137	85	52		
Age (years)					
≤60	104 (75.9)	66 (77.6)	38 (73.1)	0.369	0.544
>60	33 (24.1)	19 (22.4)	14 (26.9)		
Sex					
Male	103 (75.2)	66 (77.6)	37 (71.2)	0.729	0.393
Female	34 (24.8)	19 (22.4)	15 (28.8)		
BMI					
<28	101 (73.7)	62 (72.9)	39 (75.0)	0.071	0.79
≥28	36 (26.3)	23 (27.1)	13 (25.0)		
T stage					
T1	111 (81.0)	75 (88.2)	36 (69.2)	7.578	0.006
T2-T4	26 (19.0)	10 (12.8)	16 (30.8)		
N stage					
N1	6 (4.4)	1 (1.2)	5 (9.6)	3.656	0.056
N0	131 (95.6)	84 (98.8)	47 (90.4)		
M stage					
M1	13 (9.5)	2 (2.4)	11 (21.2)	13.278	<0.001
M0	124 (90.5)	83 (97.6)	41 (78.8)		
AJCC stage					
I-II	113 (82.5)	82 (96.5)	31 (59.6)	30.328	<0.001
III-IV	24 (17.5)	3 (3.5)	21 (40.4)		
WHO/ISUP Grade					
I-II/Low	113 (82.5)	80 (94.1)	26 (50.0)	35.867	<0.001
III-IV/High	24 (17.5)	5 (5.9)	26 (50.0)		

Values in bold font indicate statistical significance ($P < 0.05$). BMI, body mass index; T, primary tumor size; N, lymph node metastasis; M, distant metastasis; CDCA5, cell division cycle-associated 5; ccRCC, clear cell renal cell carcinoma.

concentration medium (10% FBS) into the 24-well plate, $\sim 2 \times 10^4$ cells were added to the compartments with 150 μ l medium containing 1% FBS. Following incubation for 12 h or overnight at 37°C incubator, the cells remaining on the surface above were gently removed using a cotton swab. The chamber with the migrating cells attached to the bottom surface was then fixed with methanol and stained with 0.1% crystal violet at room temperature for 20 min dye. Subsequently, the chambers were screened, imaged and quantified in five random fields per well under an electronic upright microscope (Eclipse Ts2R, Nikon Corporation). All assays were performed independently three times.

Western blot analysis. Total protein from tissues and cells were isolated using RIPA lysis buffer containing protease inhibitor cocktail (#5871, Cell Signaling Technology, Inc.). The BCA method was utilized for protein quantification. The quantified protein (30 μ g) was separated by 8-12% SDS/PAGE gel electrophoresis, and then transferred onto 0.45 polyvinylidene fluoride membranes (Direct-Q, MilliporeSigma). After

blocking the membranes with 5% non-fat milk for 1 h at room temperature, they were incubated with the respective primary antibodies overnight at 4°C. The primary antibodies used were as follows: Anti-CDCA5 (1:2,000, cat. no. ab192237, Abcam), β -tubulin (1:3,000, cat. no. BE0025, Easy Bio, Inc.), Akt (11E7, 1:2,000, cat. no. 4685S, Cell Signaling Technology, Inc.), phosphate Akt (Ser473, 1:2,000, cat. no. 4060S, Cell Signaling Technology, Inc.), Stat3 (D3Z2G, 1:2,000, cat. no. 12640S, Cell Signaling Technology, Inc.), phosphorylated (p)-Stat3 (Tyr705, 1:2,000, cat. no. 9145S, Cell Signaling Technology, Inc.), NF- κ B (1:1,000, cat. no. BE3154, Easy Bio, Inc.), p-NF- κ B (1:2,000, cat. no. 3033S, Cell Signaling Technology, Inc.), mTOR (1:5,000, cat. no. 66888-1-Ig, ProteinTech Group, Inc.), p-mTOR (Ser2448, 1:2,000, cat. no. 5536, Cell Signaling Technology, Inc.), p- γ -H2A histone family member X (γ -H2AX; Ser139, 1:1,000, cat. no. 9718T, Cell Signaling Technology, Inc.), breast cancer type 1 (BRCA1; 1:1,000, cat. no. 14823S, Cell Signaling Technology, Inc.), p-BRCA1 (Ser1524, 1:1,000, cat. no. 9009, Cell Signaling Technology, Inc.), cyclin B1 (1:1,000, cat. no. 55004-1-AP, ProteinTech

Group, Inc.), poly(ADP-ribose) polymerase (PARP; 46D11, 1:1,000, cat. no. 9532, Cell Signaling Technology, Inc.), Bcl-2 (Ser2448, 1:1,000, cat. no. 12789-1-AP, ProteinTech Group, Inc.). The membranes were then incubated with horseradish peroxidase (HRP)-conjugated secondary antibodies diluted in antibody dilution buffer (A1810, Solarbio) for 1 h at room temperature and visualized using the ECL system (Thermo Fisher Scientific, Inc.). The secondary antibodies used were as follows: Anti-rabbit IgG HRP-linked antibody (1:5,000, cat. no. 7074, Cell Signaling Technology, Inc.) and anti-mouse IgG HRP-linked antibody (1:5,000, cat. no. 7076, Cell Signaling Technology, Inc.). The bands were quantified using the Tanon Gel Image System (Tanon-5200, Biotanon, Shanghai, China).

Reverse transcription-quantitative polymerase chain reaction (RT-qPCR). The cells and tissues were lysed using TRIzol[®] reagent (Invitrogen; Thermo Fisher Scientific, Inc.). Total RNA was extracted using chloroform extraction, as well as isopropanol precipitation. Reverse transcription was then conducted using a cDNA synthesis kit (E6560S, New England Biolabs) at 42°C for 15 min. Subsequent quantitative polymerase chain reaction (qPCR) analyses for each cDNA genes were quantified under specific conditions as follows: The qPCR program consisted of pre-denaturation at 94°C for 30 sec, followed by 40 amplification cycles of denaturation (94°C for 5 sec), annealing (50°C for 15 sec) and extension (72°C for 10 sec). The reactions were performed on an ABI 7500 Fast Real-Time PCR System (Applied Biosystems; Thermo Fisher Scientific, Inc.). *Homo sapiens* peptidylprolyl isomerase A (PPIA) was applied as an internal reference gene. The validated primers used were as follows: CDCA5 forward, 5'-GAGGTCCCAGCGGAAATCAG-3' and reverse, 5'-TCTTTAAGACGATGGGCTTTC TG-3'; PPIA forward, 5'-GTGTTCTTCGACATTGCCGTC-3' and reverse, 5'-TGCACGATCAGGGGTAAACA-3'. The data were calculated using the $2^{-\Delta\Delta C_q}$ method (18).

Flow cytometry. To detect the cell cycle, the 786-O and SN12-PM6 cells transfected with lentivirus for 24 h followed by puromycin treatment for 48 h, were collected and fixed in cold 95% ethanol for 3 h at 4°C, then washed with phosphate-buffered saline (PBS) and treated with propidium iodide (PI) staining solution (CA1020, Beijing Solarbio Science & Technology Co., Ltd.) for 30 min according to the manufacturer's instructions. The analysis of cell apoptosis was performed using the FITC Annexin V apoptosis detection kit (CA1020, Beijing Solarbio Science & Technology Co., Ltd.) according to the manufacturer's instructions. A BD FACSCalibur (BD Biosciences) flow cytometer was used to analyze percentage of the cells in each cell cycle phase and apoptosis.

Tissue microarray (TMA) and immunohistochemistry (IHC). TMAs containing 137 paired formalin-fixed paraffin-embedded (FFPE) ccRCC and adjacent normal tissue samples were constructed. IHC for CDCA5 expression in the TMAs was carried out using a standard protocol (19). The tissue microarray was constructed manually and a 2-mm cylindrical core sample from tissue donor blocks (for cohort please see Table I) was placed in a prepared 6x10 array of recipient wax blocks with a 1.5-mm hole spacing. The recipient wax block was arranged with a maximum of 30 matched pairs of tumor

and adjacent tumor tissues. Paraffin-embedded 5- μ m-thick tissue sections were deparaffinized by the following steps: 10 min in xylol twice, 5 min in 100% ethanol twice, and 90, 80, and 70% ethanol for 5 min each. Then those sections were placed in 10 mM citric acid buffer for antigen retrieval and boiled it using a microwave at 100°C for 15 min. The slides were then incubated with rabbit anti-CDCA5 antibody overnight at a dilution of 1:200 at 4°C, followed by incubation with secondary anti-rabbit antibody (PV-9001, OriGene Technologies, Inc.) at room temperature. Each TMA spot and IHC slides were photographed using TissueFAXS imaging system (TissueGnostics GmbH) and evaluated by its intensity of staining: 0 (no staining, negative), 1 (<10% of malignant cells staining, weak positive), 2 (10-50% of malignant cells staining, moderate positive), or 3 (>50% of malignant cells staining, strong positive).

Furthermore, IHC was performed on the paraffin-embedded tumors harvested from orthotopic xenografts in nude mice to investigate the expression of Ki67, caspase-3, and γ -H2AX in the shCDCA5 group and control group. IHC was conducted by the steps and conditions mentioned above. The primary antibody and dilution for incubation were Ki67 (D3B5, 1:400, cat. no. 12202, Cell Signaling Technology, Inc.), caspase-3 (1:1,000, cat. no. 9662, Cell Signaling Technology, Inc.) and γ -H2AX (Ser139, 1:480, cat. no. 9718T, Cell Signaling Technology, Inc.).

Orthotopic RCC tumorigenicity in nude mice. The scientific use of orthotopic animal models was conducted between December, 2020 to January, 2021. Due to the control policy of the coronavirus disease 2019, the animal center at our institution was temporarily suspended and the authors could only resort to other authorized animal centers to perform the animal experiments. The use of animals was approved (approval no. ACU20-245) by the Institutional Animal Care and Use Committee (IACUC) of Cyagen Biosciences (Jiangsu, China). The study was performed under the supervision and inspection of the committee and the Cyagen Research Centre for model organisms. BALB/c nude immunodeficient male mice (4 to 6 weeks old) were obtained from Vital River Laboratory Animal Technology Co. Ltd. These BALB/c mice were housed under specific-pathogen-free conditions at a room temperature of 23 \pm 2°C and 50-60% humidity under a 12/12-h light/dark cycle with food and water provided *ad libitum*. A total of 12 BALB/c nude mice were included and randomly divided into the shCDCA5 group and control group. Prepared cells (3x10⁵) subjected to stable CDCA5 knockdown or those transfected with the empty vector were suspended in PBS with Matrigel (Corning, Inc.). The mice were anesthetized by an intraperitoneal injection of sodium pentobarbital (30 mg/kg) and the cells were then orthotopically implanted into the right subrenal capsule (n=6 mice in each group). A total of 8 mice were eventually included in the analysis as the other 4 mice were subjected to euthanasia at an early stage due to surgery-related adverse complications and a body weight loss of >20%. Euthanasia was performed using an intravascular administration of an overdose of sodium pentobarbital (>100 mg/kg) followed by cervical dislocation. Euthanasia was confirmed by the loss of vital signs, such as respiration and heartbeat cessation. Diagnostic bioluminescence imaging, as

well as animal weight data were collected on a weekly basis to monitor tumor development during the experiment. For dynamic bioluminescence imaging, D-luciferin potassium salt (2591-17-5, ApexBio) was prepared at a concentration of 15 mg/ml. The mice were then anesthetized and intraperitoneally injected with D-luciferin (10 μ l/g). After the injection for 10 min, these mice were placed into the imaging chamber to quantitatively assess tumor burden per week (days 7, 14 and 21). The D-luciferase intensity was evaluated using a bioluminescent imaging system (NightOWL II LB 983, Berthold). As regards the total burden of tumor expansion and distress on animal welfare, the mice were euthanized by overdose of sodium pentobarbital (>100 mg/kg) followed by cervical dislocation at the third week, which was the earliest stage at which a scientific decision could be made. Tumor volume calculations were obtained using the following formula: $V=1/2 \times \text{length} \times \text{width}^2$, where 'length' represents the longest dimension and 'width' represents the widest dimension (20). In all harvested tumors, the maximum tumor volume was 3.83 cm³ and the maximum tumor size was 1.40 cm.

To assess morphologic changes in orthotopic tumor growth, hematoxylin and eosin (H&E) staining were conducted. Hematoxylin and eosin staining kits (G1120, Beijing Solarbio Science & Technology Co., Ltd.) were used according to instruments. The harvested tumor from the mice were formalin-fixed, paraffin-embedded, and cut into 5- μ m-thick tissue sections. Deparaffinization and hydration followed the same steps as IHC. The slides were then stained at room temperature in hematoxylin for 2 min, differentiated in 1% acid alcohol for 3 sec, washed in running water for 5 min, and then counterstained with 1% eosin for 1 min. Following dehydration and mounting, the slides were photographed using the TissueFAXS imaging system (TissueGnostics GmbH).

Immunofluorescence (IF) analysis with a confocal microscope. The 786-O and SN12-PM6 cells were each cultured in three wells of a 24-well plate with coverslips. Following transfection with lentivirus for 24 h and screening with puromycin for a further 48 h, the cells were fixed and then blocked in 3% goat serum albumin-PBS. Primary antibody against γ -H2AX (1:100, 9718s, Cell Signaling Technology, Inc.) and p-histone H3 (Ser10, 1:800, cat. no. 3377, Cell Signaling Technology, Inc.) was incubated with the cells overnight at 4°C. The cells were then washed and incubated with Alex Fluor 594 goat anti-rabbit IgG (1:500, A32740, Invitrogen; Thermo Fisher Scientific, Inc.) for 1 h at room temperature. The coverslips were then placed on fluorescent mounting medium with DAPI (ZLI-9557, OriGene Technologies, Inc.) and incubated at room temperature. The slides were imaged using a Leica SP5 confocal microscope (Leica Microsystems GmbH) at x100 magnification and analyzed using software (Leica LAS AF Lite 2.6; Leica Microsystems CMS GmbH).

Statistical analysis. Data are generally expressed as the mean \pm standard deviation (SD) from experiments independently performed at least three times. The Wilcoxon matched-pairs signed rank test was used to investigate differences in the relative mRNA levels between the patient groups. The Chi-squared test was applied to analyze the associations

between CDCA5 expression levels and the patient clinicopathological characteristics, while the continuity correction of the Chi-squared test was applied to variables of the N stage and M stage. The Student's t-test was used for the comparison between the two groups. Measurement data between three or more groups were analyzed using one-way ANOVA followed by Tukey's post hoc test. Overall survival (OS) analysis was performed using Kaplan-Meier analysis and further comparisons were made using log-rank tests. The Cox proportional hazards regression model was applied to identify the risk factors. Statistical calculations were performed using SPSS 23.0 software (SPSS Inc.).

Results

Clinicopathological characteristics and upregulated CDCA5 expression indicate an aggressive status of ccRCC. To evaluate CDCA5 expression patterns in 33 TCGA cancer types, a comprehensive examination of TCGA mRNA database was conducted. The boxplot comparing tumor and normal tissue CDCA5 expression revealed that CDCA5 was overexpressed in the majority of malignancies (Fig. 1A). TCGA online analysis revealed that CDCA5 expression was upregulated in primary ccRCC tumors compared with adjacent normal tissue (Fig. 1B). The increased expression of CDCA5 was positively associated with the Fuhrman grade, advanced TNM stages and lymph node metastasis (Fig. 1C-E), indicating an expression dependency on aggressive status in ccRCC.

Patients with a highly expression of CDCA5 had a poorer prognosis (Fig. 2A). In addition, a survival probability analysis was performed combining the CDCA5 expression level and tumor grade for patients with ccRCC (Fig. 2B). Patients with a low/medium CDCA5 level with grade 1 tumors (Fig. 2B, upper blue line) exhibited a tendency for an improved survival, whereas patients with a high CDCA5 expression with grade 4 tumors had the worst OS (Fig. 2B, lower green line). Thus, the combination of the CDCA5 expression status and tumor grade had a strong predictive value for survival outcomes. To explore the diagnostic value of CDCA5 in predicting prognosis, the association between the GSVA score and clinical survival in all the 33 TCGA cancers was estimated. It was demonstrated that CDCA5 in patients with ccRCC with a higher GSVA score could effectively be utilized as a hazard predictor for OS [hazard ratio (HR), 1.83; $P<0.001$], progression-free survival (HR, 1.74; $P<0.001$) and disease-specific survival (HR, 3.15; $P<0.001$) (Fig. 2C).

To investigate the malignant impact of CDCA5, western blot analyses of cultured human ccRCC cell lines was performed and the results revealed a higher CDCA5 expression in the ccRCC cell lines, particularly in the 786-O and SN12-PM6 cell lines (Fig. 3A). As regards the ccRCC tissues, RT-qPCR was performed to quantify the mRNA expression levels in 21 resected paired tumor and adjacent normal tissues. It was found that CDCA5 was overexpressed in ccRCC samples (Fig. 3B).

Furthermore, the protein expression characteristics of four different tumor stages were validated using another paraffin-embedded paired tissues from patients with 137 ccRCC from Chinese PLA General Hospital using IHC in a TMA (Fig. 3C). The IHC score of CDCA5 expression

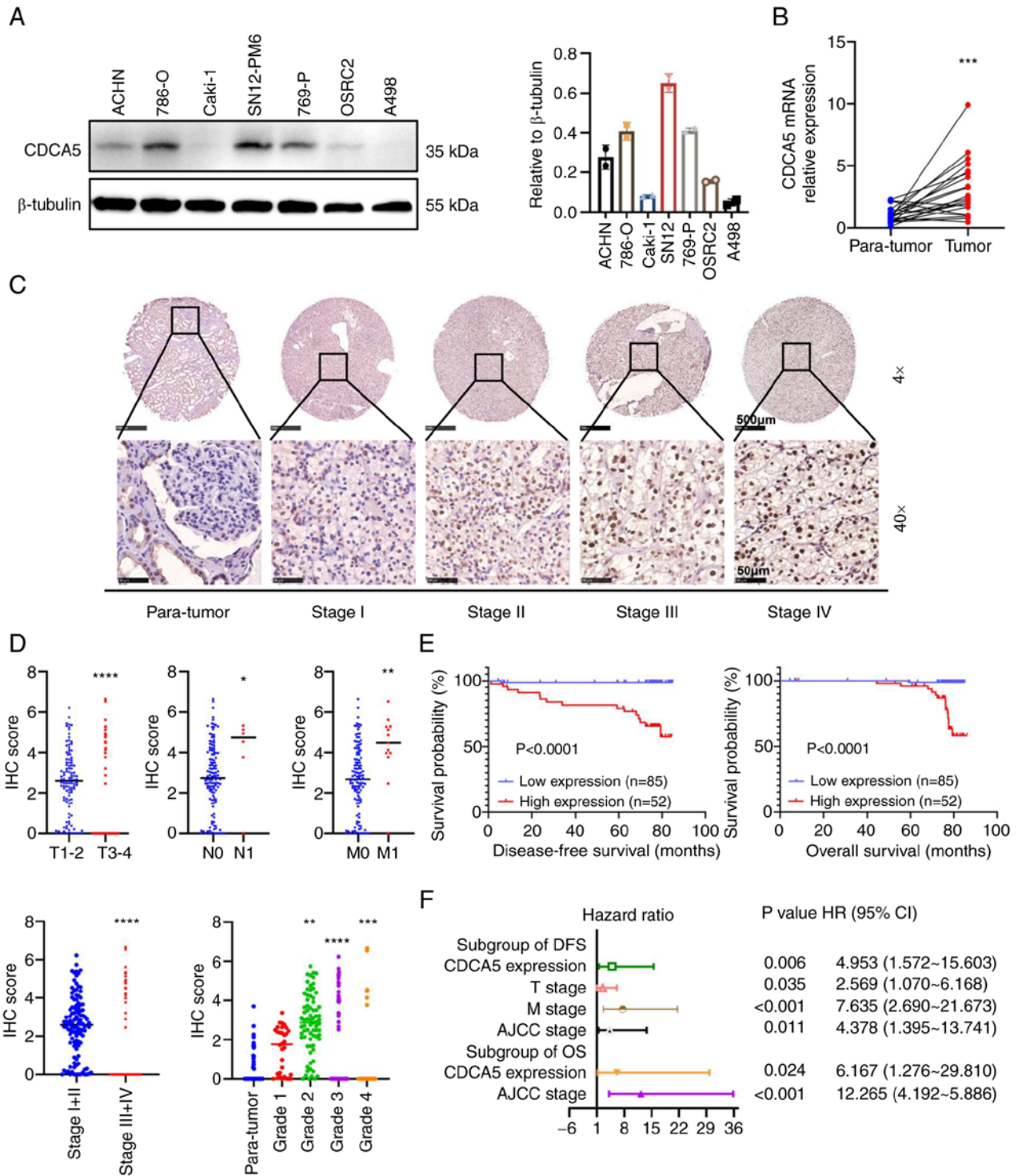


Figure 3. Relative CDCA5 expression in renal cancer cell lines and tissues with its survival significance. (A) Protein expression of CDCA5 in renal cancer cell lines examined using western blot analysis. (B) Relative mRNA expression of CDCA5 in 21 pairs of ccRCC tissues and adjacent tissues examined using reverse transcription-quantitative PCR. (C) Representative tissue microarray stained for CDCA5 in 137 patients with ccRCC. The immunoreactivity of CDCA5 expression in ccRCC and normal tissues was analyzed based on different cancer stages. Upper panels: Magnification, $\times 4$; scale bar, $500 \mu\text{m}$; lower panels: Magnification $\times 40$; scale bar, $50 \mu\text{m}$. (D) IHC score of CDCA5 expression was significantly higher in ccRCC tissues with an advanced T stage, positive lymphatic metastasis, distant metastasis, higher TNM stage, and elevated pathological grade. The IHC score was quantified according to the integrated optical density per field. (E) Kaplan-Meier survival analysis indicated a poor OS and DFS of patients with ccRCC with a high CDCA5 expression. (F) Forest plot of hazard ratios for DFS and OS. Multivariate cox regression model of prognostic factors is displayed with 95% CI values. * $P < 0.05$, ** $P < 0.01$, *** $P < 0.001$ and **** $P < 0.0001$ vs. para-tumor tissue. CDCA5, cell division cycle-associated 5; ccRCC, clear cell renal cell carcinoma; IHC, immunohistochemistry; DFS, disease-free survival; OS, overall survival.

quantified by integral optic density (IOD) values demonstrated that CDCA5 staining was intensified along with an elevated T stage, lymph node metastasis, distant metastasis, an elevated

AJCC stage and an advanced WHO/ISUP grade in ccRCC tissues (Fig. 3D). Accordingly, a strong association between a high CDCA5 expression and the clinical characteristics of

patients with ccRCC was observed for characteristics such as primary tumor size ($P=0.006$), distant metastasis ($P<0.001$), AJCC stages ($P<0.001$) and WHO/ISUP grade ($P<0.001$) (Table I). These data were in accordance with those from TCGA dataset analysis.

Moreover, with a follow-up time of 76.933 ± 0.372 months, Kaplan-Meier survival analysis revealed that a high expression of CDCA5 was associated with a poorer 5-year disease-free survival (DFS) and a worse OS (Fig. 3E). Multivariate cox regression stepwise analysis (Table SI) (the significant factors are displayed as a forest plot; Fig. 3F), confirmed that a high CDCA5 expression remained an independent risk factor both for both OS [$P=0.024$; HR, 6.167; 95% confidence interval (CI), 1.276-29.810] and DFS ($P=0.006$; HR, 4.953; 95% CI, 1.572-15.603). The AJCC stage was also a hazardous factor for both DFS ($P=0.011$; HR, 4.378; 95% CI, 1.395-13.741) and OS ($P<0.001$; HR, 12.265; 95% CI, 4.192-5.886).

Collectively, these results confirm that CDCA5 expression and AJCC stage may serve as malignant prognostic factors for the OS and DFS of patients with ccRCC.

CDCA5 knockdown inhibits the proliferation and migration of ccRCC cells. Since TCGA analysis indicated that the expression of CDCA5 was associated with ccRCC progression and nodal metastasis, the present study then investigated the biological function of CDCA5 in ccRCC cell lines. After transfecting shRNA targeting CDCA5 and negative control shRNA into the SN12-PM6 and 786-O cells. Western blot analyses confirmed the decreased protein expression of CDCA5 in SN12-PM6 and 786-O cells transfected with shRNA lentivirus (Fig. 4A).

The knockdown of CDCA5 significantly hindered cell proliferation. Cell viability was markedly decreased in both cell lines, as shown using crystal violet assay ($P<0.01$; Fig. 4B). As CDCA5 significantly affected ccRCC cell proliferation, its effects on migration were thus evaluated. Transwell assays demonstrated that the knockdown of CDCA5 impaired the cell migratory ability *in vitro* compared with the control group (Fig. 4C). Thus, CDCA5 is vital to maintain ccRCC cell proliferative and migratory ability.

CDCA5 knockdown induces cell cycle arrest in the G2/M phase. To further investigate the underlying mechanisms of the inhibitory effects of CDCA5 on cell proliferation, cell cycle analysis was performed to the effects of CDCA5 knockdown on the cell cycle. Flow cytometric analyses revealed that CDCA5 knockdown decreased cell distribution in the G0/G1 phase, while increasing the cell proportion in the G2/M phase in both the SN12-PM6 and 786-O cell lines ($P<0.05$; Fig. 5A). Moreover, the IF analysis of p-histone 3 demonstrated a decreased number of positive cells in the shCDCA5 groups compared with the increasing positive ratio in the NC group (Fig. 5B). Moreover, a decreased cyclin B1 expression were observed using western blot analysis in both the 786-O and SN12-PM6 cell lines following the knockdown of CDCA5 (Fig. 5C), which suspended cell cycle progression into mitosis. As a result, this G2/M arrest eventually inhibited tumor cell proliferation. These data confirm that CDCA5 has a regulatory function in the cell cycle in the G2/M checkpoint.

CDCA5 knockdown improves DDR. As CDCA5 is required for sister chromatid cohesin to maintain genome stability (6), the present study further validated whether the knockdown of CDCA5 could trigger DDR. The phosphorylation of H2AX, which is a biomarker of double strand breaks, was found to increase the numbers of foci formation in IF following the knockdown of CDCA5 in the 786-O (Fig. 6A) and SN12-PM6 (Fig. 6B) cells. Furthermore, a large proportion of γ -H2AX-positive cells in both cell lines was found in the shCDCA5 groups ($P<0.01$). The increased expression of γ -H2AX in the cells in which CDCA5 was knocked down was also detected using western blot analysis (Fig. 6C). Moreover, the expression of the DNA damage repair gene, BRCA1 and p-BRCA1, was decreased following CDCA5 knockdown, indicating the further abrogation of the ability to repair DNA. Taken together, these findings indicate that the knockdown of CDCA5 triggers the sequential activation of the DDR and abrogates the repair of damaged DNA.

CDCA5 knockdown promotes apoptosis and regulates ccRCC behavior via the DDR. As a response to DNA damage and cell cycle arrest, the present study then investigated the cell fate towards apoptosis. The effects of CDCA5 on cell apoptosis were analyzed using flow cytometry with Annexin V-FITC staining. The results demonstrated that CDCA5 knockdown promoted both early and late apoptosis in the shCDCA5 groups compared with the control groups. Late apoptosis was prominent according to the flow cytometric analysis ($P<0.001$; Fig. 7A). In the 786-O cells, the average percentage of apoptotic cells (early and late apoptosis) in the shCDCA5-1 group was increased 3.3-fold, while this was increased 1.6-fold in the shCDCA5-2 group. In the SN12-PM6 cells, the total number of apoptotic cells in the shCDCA5-1 group was increased 5.2-fold, while this was increased 4.1-fold in the shCDCA5-2 group, compared with the control (Fig. 7A).

Consistently, the levels of cell apoptosis-related proteins levels were examined using western blot analysis. The knockdown of CDCA5 notably decreased the expression of the anti-apoptotic protein, Bcl-2. The levels of downstream proteins, such as PARP were activated; the expression of cleaved PARP was increased following CDCA5 knockdown (Fig. 7B).

Tumor-promoting inflammation is an enabling characteristic, and damaged DNA can contribute to the crosstalk between inflammation and the immune response in cancer (21,22). In the present study, to investigate the potential inflammation pathways triggered by DDR following the knockdown of CDCA5, western blot analysis was performed. The prominent change observed was in the levels of the transcription factors, Stat3 and NF- κ B, related to the inflammatory response. It was observed that the Stat3, p-Stat3, NF- κ B and p-NF- κ B expression levels were decreased following CDCA5 knockdown (Fig. 7B). Moreover, the expression of total mTOR, p-mTOR, total AKT, and p-AKT was decreased in the cells transfected with shCDCA5-1 and shCDCA5-2 (Fig. 7B). The inhibition of the AKT/mTOR signaling pathway can suppress the inflammatory response. Taken together, the knockdown of CDCA5 predominantly activated the DDR, promoted apoptosis and decreased the expression of STAT3, NF- κ B, mTOR and AKT to reduce tumor malignancy.

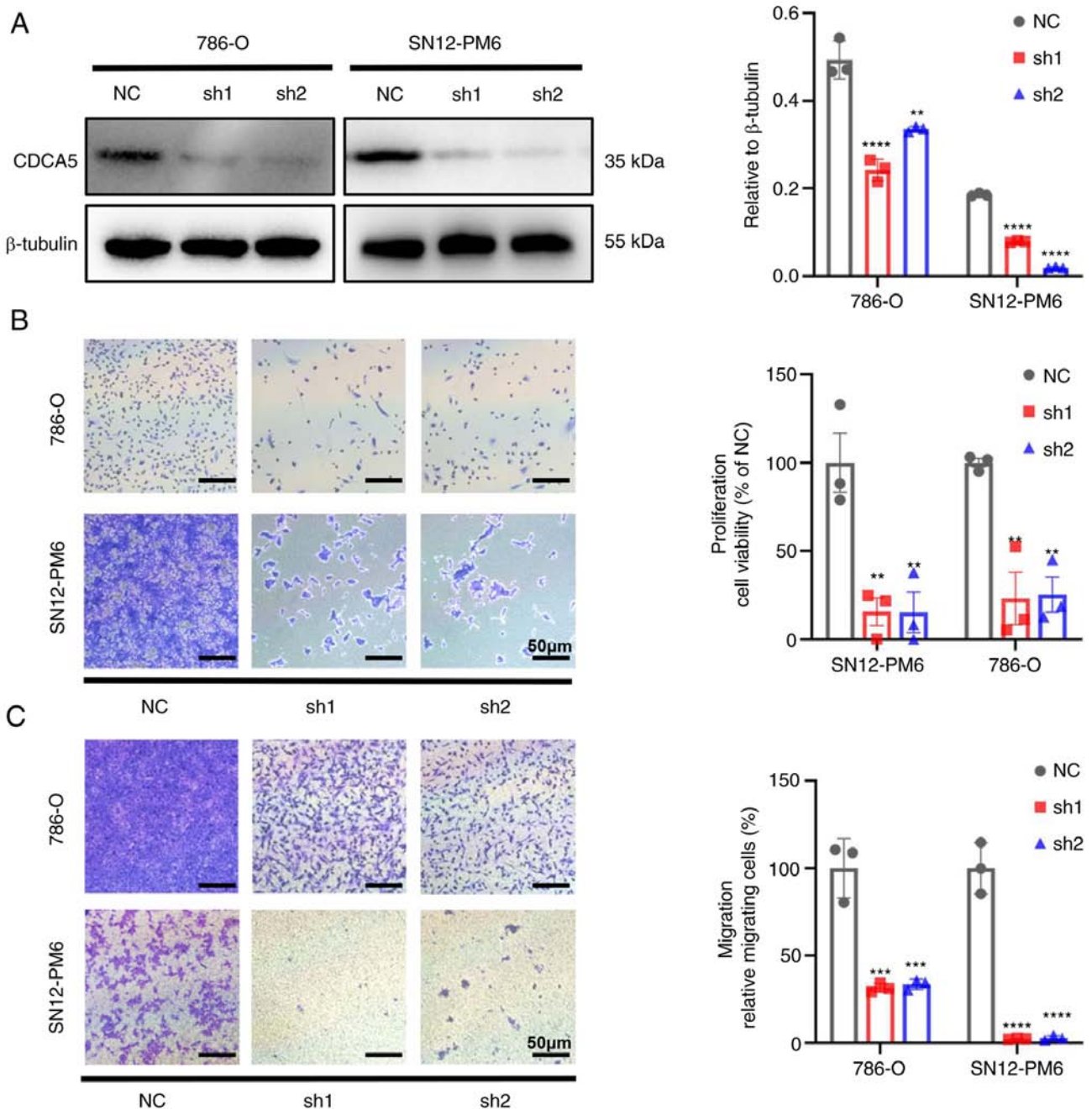


Figure 4. CDCA5 knockdown inhibits the proliferation and migration of ccRCC cells *in vitro*. (A) Knockdown efficiency of CDCA5 in SN12-PM6 and 786-O cells following transfection was confirmed using western blot analysis. (B) CDCA5 knockdown reduced cell proliferation as shown by crystal violet staining. The viability rate of cells=(the OD values of treated groups/the OD values of the NC group) \times 100%. Scale bar, 50 μ m. (C) CDCA5 knockdown significantly suppressed the migration of SN12-PM6 and 786-O cells. Scale bar, 50 μ m. Data are presented as the mean \pm standard deviation from three independent experiments. ** P <0.01, *** P <0.001 and **** P <0.0001 vs. negative control. CDCA5, cell division cycle-associated 5; ccRCC, clear cell renal cell carcinoma; NC, negative control.

CDCA5 knockdown suppresses tumorigenesis in an orthotopic model of RCC. To illuminate the function of CDCA5 in tumorigenicity *in vivo*, luciferase-expressing SN12-PM6 cells transfected with shCDCA5 or NC lentivirus were prepared and injected orthotopically into the right kidneys of nude mice. Intratumoral green fluorescent protein (GFP) fluorescence was detected following the administration of D-luciferin at 4 weeks in the xenograft model. A strong luciferase signal was obtained in the mice implanted with cells transfected with the control vector, whereas a reduced signal intensity was observed in the shCDCA5

group (Fig. 8A). Moreover, SN12-PM6 xenografts transfected with shCDCA5 exhibited a significantly decreased tumor growth, with a decreased tumor volume and weight (Fig. 8B).

To determine the effects of CDCA5 inhibition on DDR and tumor cell apoptosis in tumor xenografts, tumors were resected and embedded for H&E staining and IHC (Fig. 7C). IHC analysis confirmed that tumors derived from cells in which shCDCA5 was knocked down displayed a significantly decreased Ki67 expression compared with the control tumors (P <0.05; Fig. 8C). Moreover, the knockdown of CDCA5

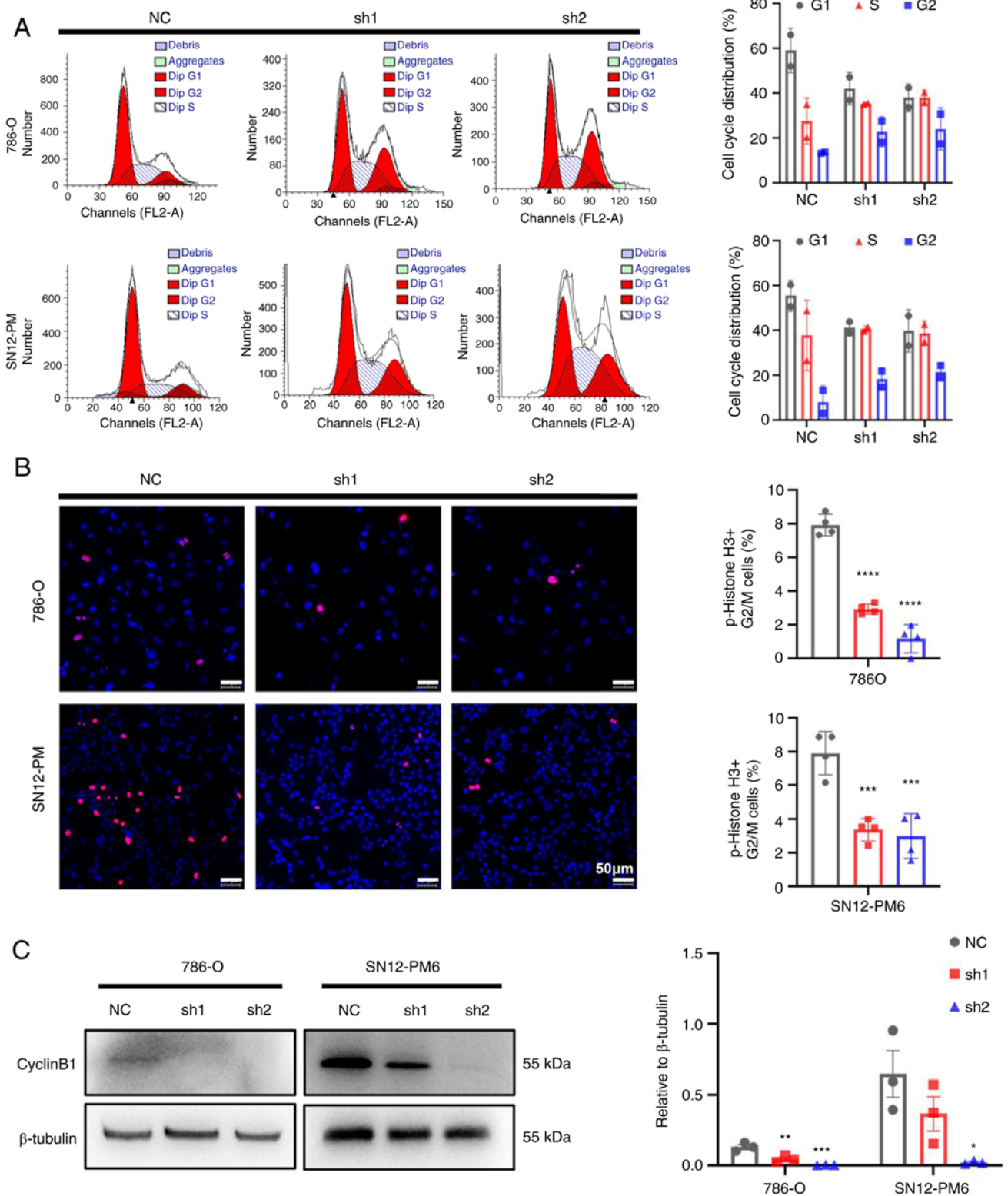


Figure 5. Knockdown of CDCA5 induces cell cycle arrest in the G2/M phase. (A) Knockdown of CDCA5 increased the cell population in the G2 phase, but decreased the number of cells in the G1 phase, as shown by flow cytometric analysis in 786-O and SN12-PM6 cells. (B) Immunostaining analysis using the mitotic marker p-histone H3 (Serine 10; red) revealed a marked decrease in the number of positive cells in the shCDCA5 group. Nuclear DNA (blue) was stained with DAPI. (C) Western blot analysis of cyclin B1 in both 786-O and SN12-PM6 cell lines following the knockdown of CDCA5. Scale bars, 50 μ m. * P <0.05, ** P <0.01, *** P <0.001 and **** P <0.0001 vs. negative control. CDCA5, cell division cycle-associated 5; NC, negative control.

significantly promoted γ -H2AX accumulation (P <0.05; Fig. 8C), confirming the potential pivotal role of CDCA5 in DDR. Caspase-3 expression was upregulated in the shCDCA5 group. This revealed the induction of cell apoptosis *in vivo*

(P <0.001; Fig. 8C). Thus, the orthotopic model demonstrated that shCDCA5 knockdown significantly suppressed tumor proliferation and growth *in vivo* through the induction of DDR and apoptosis.

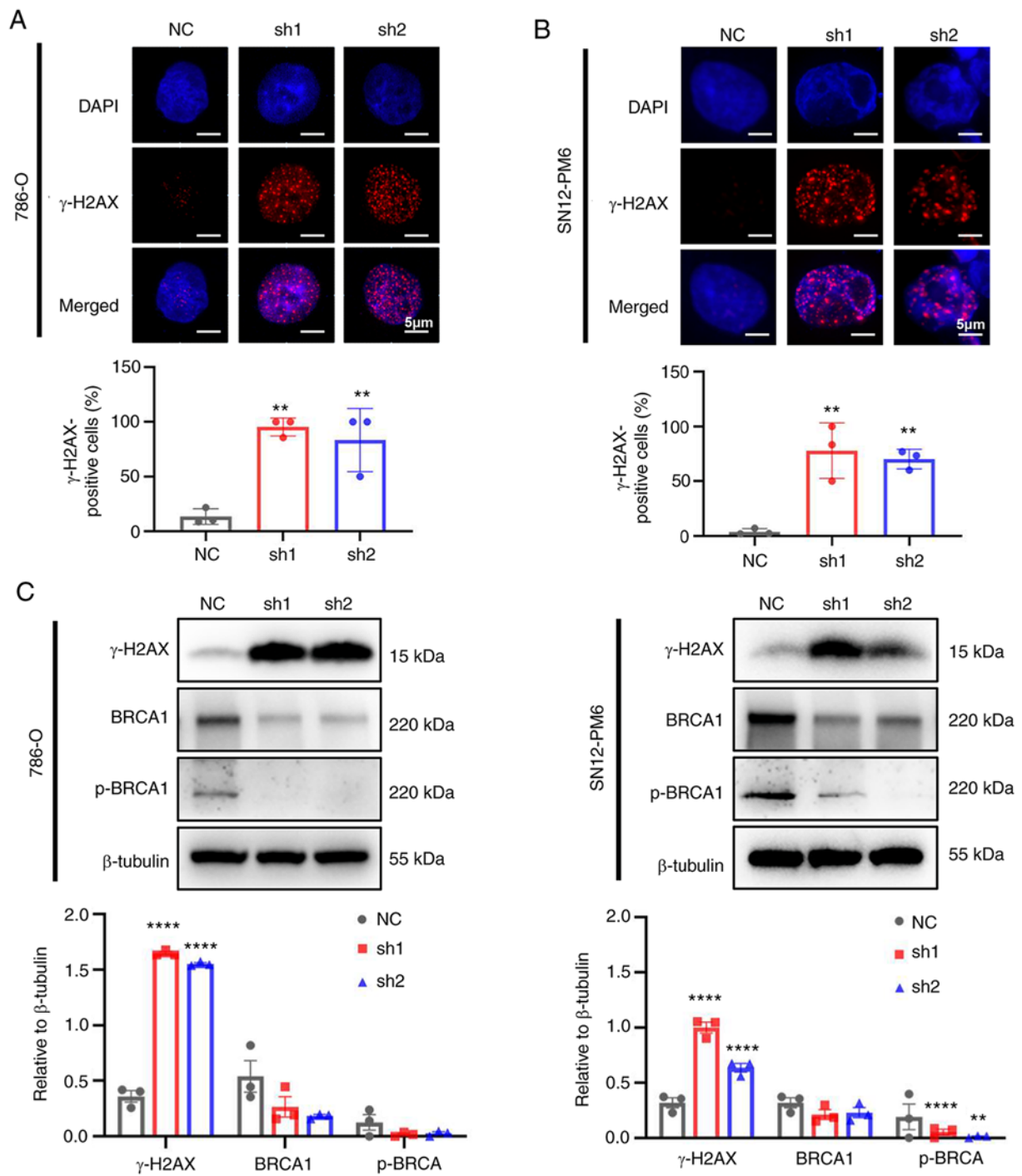


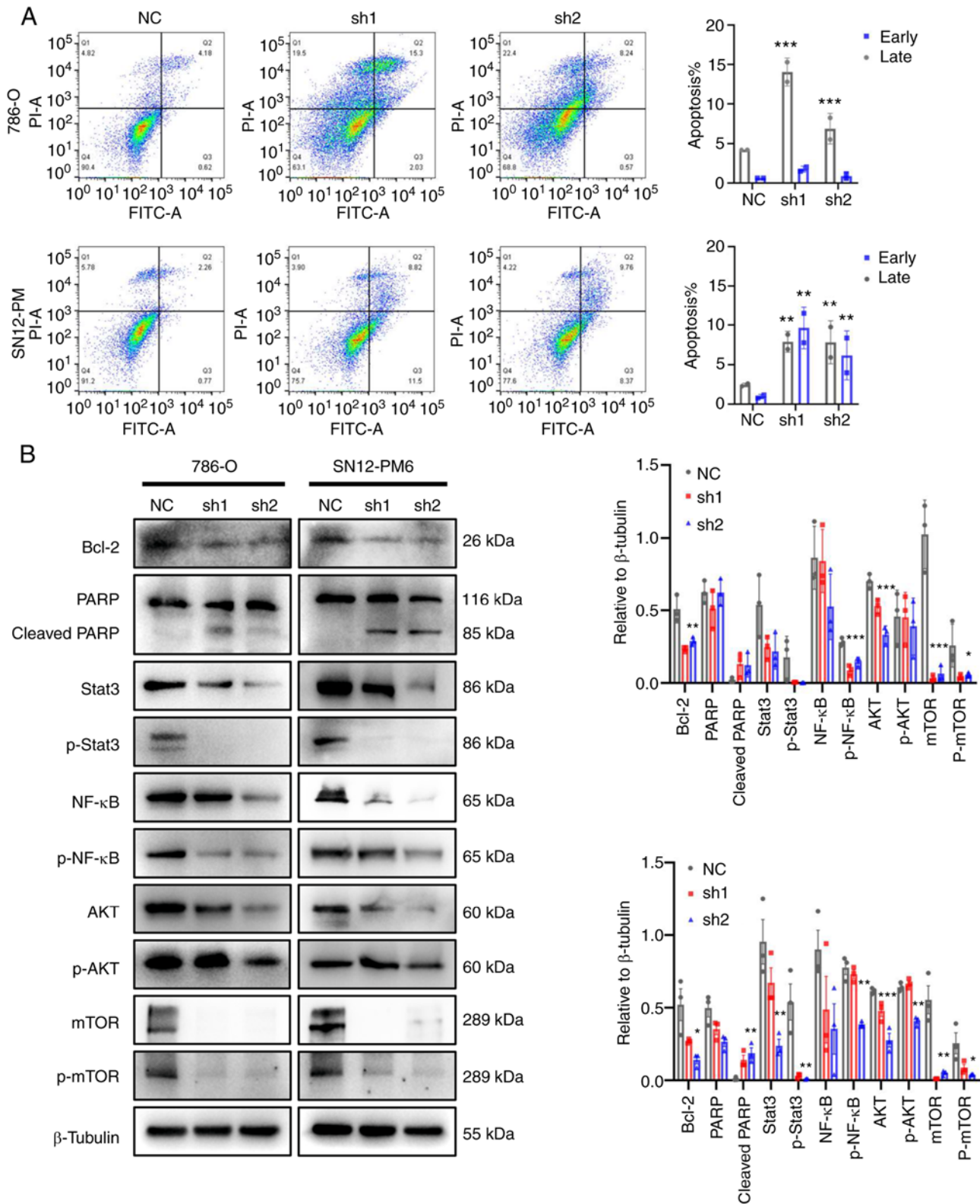
Figure 6. CDCA5 knockdown induces the DNA damage response. (A) Immunofluorescence staining revealed increased γ -H2AX foci (red) formation in 786-O cells following CDCA4 knockdown and an increased percentage of γ -H2AX-positive cells. (B) γ -H2AX foci (red) formation increased in SN12-PM6 cells following CDCA4 knockdown and the percentage of γ -H2AX-positive cells also increased. (C) Western blot analysis of proteins related to the DNA damage response following CDCA4 knockdown in both 786-O and SN12-PM6 cell lines. Scale bars, 5 μ m. Data are presented as the mean \pm standard deviation. ** $P < 0.01$ and **** $P < 0.0001$ vs. negative control. CDCA5, cell division cycle-associated 5; NC, negative control; γ -H2AX, γ -H2A histone family member X; BRCA1, breast cancer type 1.

Discussion

With the increasing prevalence of urological cancer, ccRCC still lacks reliable biomarkers and has a refractory response to various chemotherapeutics. The development of genomic instability is one of enabling characteristics of cancer (22), which is frequently induced by gene alterations in DNA damage repair and chromatin remodeling (23). In addition, cohesin, with its

essential substrate, CDCA5, regulates chromatin segregation in metaphase-to-anaphase transition, maintains genomic stability, and drives cancer pathogenesis (24). CDCA5 has been found to be overexpressed in a number of types of cancer (16,25,26). However, to the best of our knowledge, no study to date has profiled the expression and function of CDCA5 in ccRCC.

In the present study, CDCA5 expression was found to be upregulated in ccRCC tissue and its high expression



was positively associated with a larger tumor size, distant metastasis, advanced TNM stage and a higher WHO/ISUP grade. The high expression of CDCA5 was associated with

an aggressive tumor status and a poor survival. Accordingly, univariate and multivariate Cox regression analyses identified CDCA5 overexpression as an independent indicator of

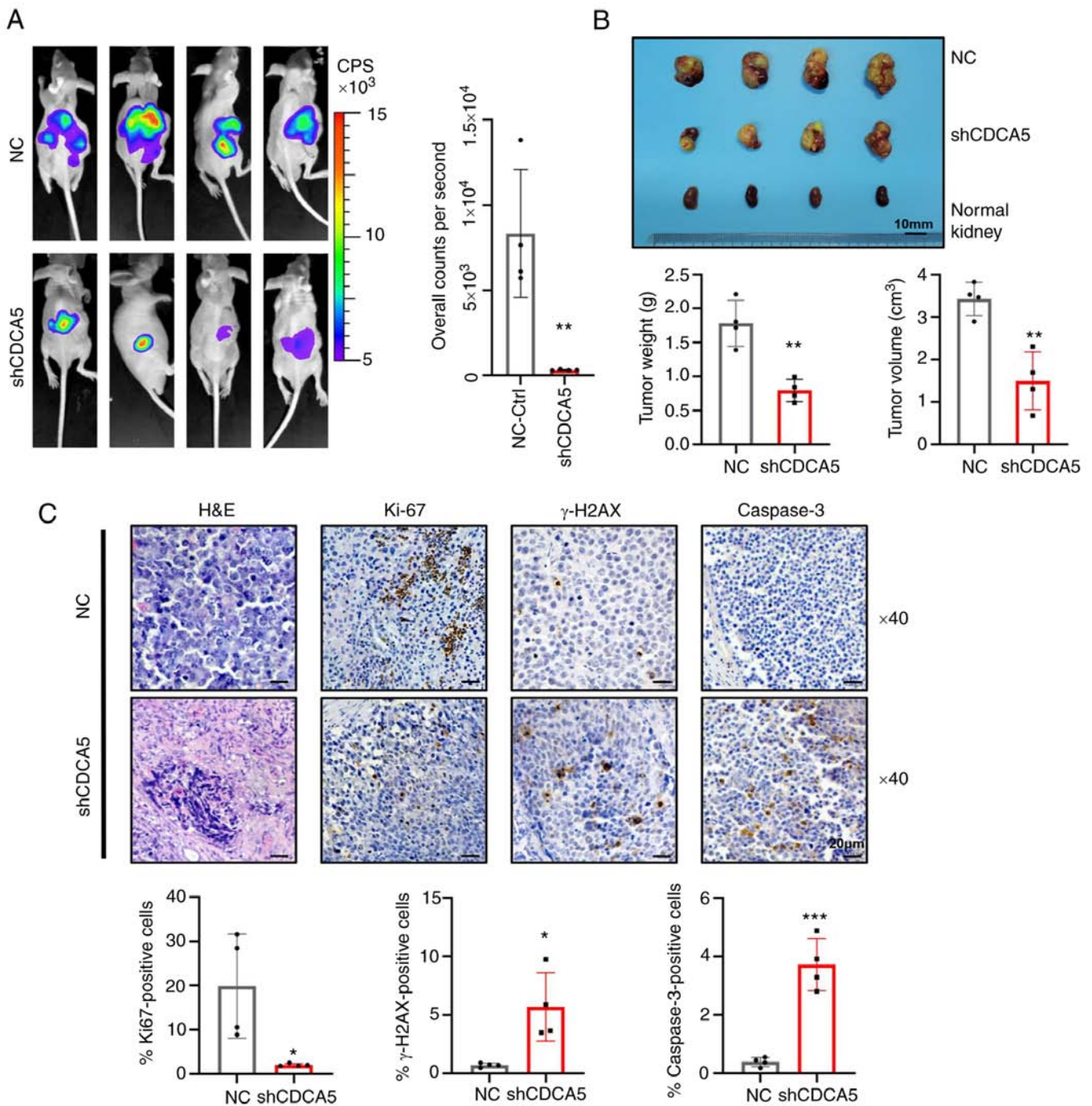


Figure 8. Knockdown of CDCA5 suppresses tumorigenesis and tumor growth of ccRCC cells *in vivo*. (A) Bioluminescence imaging by luciferase in an orthotopic ccRCC xenograft mouse model. The luciferase signaling intensity of overall counts per second was decreased in the shCDCA5 group with statistical significance. (B) The xenograft tumors were collected at 4 weeks after injection. Compared to the NC control group, tumors were smaller in the shCDCA5 group. The weight and volume of the excised xenograft tumors were analyzed between the two groups. Scale bar, 10 mm. (C) Representative graphs and quantification of H&E staining and immunohistochemistry assays for Ki67, γ -H2AX and caspase-3 in the tumor sections. Magnification, $\times 40$; scale bar, 20 μ m. * $P < 0.05$, ** $P < 0.01$ and *** $P < 0.001$ vs. negative control. CDCA5, cell division cycle-associated 5; ccRCC, clear cell renal cell carcinoma; NC, negative control; γ -H2AX, γ -H2A histone family member X.

a poorer DFS and OS. Likewise, in *in vitro* experiments, the knockdown of CDCA5 inhibited the proliferation and migration, promoted the apoptosis of SN12-PM6 and 786-O cells, and suppressed tumorigenesis in an orthotopic implantation model of ccRCC. Thus, shCDCA5 suppresses the progression and promotes the apoptosis of ccRCC cells, contributing to a beneficial outcome. Taken together, in accordance with the findings of previous studies (14,26,27),

the results of the present study support the oncogenic role of CDCA5 in ccRCC progression; thus, CDCA5 may be a possible candidate for a novel therapeutic target for selective patients with ccRCC.

The knockdown of CDCA5 markedly induced DDR. In response to DNA damage, the recruitment of γ -H2AX was enriched at sites of damage. However, the knockdown of CDCA5 markedly decreased the expression of BRCA1 and

p-BRAC1, which can abrogate the homologous repair of DNA double-strand breaks. In addition, when forced into mitosis in CDCA5-depleted cells, chromosomal fragments were observed and genome integrity was not maintained (10). In turn, difficulty to repair damaged DNA resulted in several potential tumor suppressive effects in cell proliferation inhibition, cell cycle arrest and eventually, apoptosis. As for the induction of G2/M arrest following the knockdown of CDCA5, p-histone H3, a cell cycle specific marker helped to determine the nature of cell cycle-progression manner (28). Flow cytometry and the decreased expression of p-histone-H3 in IF confirmed the presence of cell cycle arrest at the G2/M checkpoint.

Mechanistic defects in DNA repair can be exploited as potential therapeutic approaches in synthetic lethality, such as PARP inhibitors in patients carrying BRCA1/BRCA2 mutations (29). Additionally, the genome sequencing of ccRCC has revealed comprehensive mutations in tumorigenesis, including VHL, PBRM1, BAP1, etc. (3). PBRM1 is involved in the formation of the SWI/SNF chromatin remodeling complex, which facilitates DNA repair, as well as the maintenance of genomic stability (30). By antagonizing WAPL (31), the recruitment of CDCA5 is continuously required for sister chromatid cohesion maintenance, which involves DNA looping and transcriptional regulation (8,32). Molecules that are involved in DDR and chromatin remodeling may provide therapeutic strategies for ccRCC treatment.

Previous studies have demonstrated that DNA damage interacts with inflammation, activating both the innate and adaptive immune responses (33,34). Under DNA damage, one of the important pattern recognition receptors for accumulating cytosolic DNA is sensed by cyclic GMP-AMP (cGAMP) synthase (cGAS), followed by activating the stimulator of interferon genes (STING) (35). The cGAS/cGAMP/STING pathway then triggers interferon regulatory factor 3 and NF- κ B, respectively (36). Furthermore, the transcriptional production of interferons and cytokines interacts with the Stat family (37). In the present study, it was found that DDR was induced by CDCA5 knockdown; CDCA5 knockdown decreased the level of Stat3, p-Stat3, NF- κ B and p-NF- κ B that mainly weaken the inflammatory response. Correspondingly, the levels of inflammation-related factors, such as AKT and p-AKT were inactivated by CDCA5 knockdown; this finding is consistent with that of another study on bladder cancer, in which CDCA5 was shown to function through the PI3K/AKT/mTOR pathway (16). The inhibition of the AKT/mTOR and Stat3 signaling pathways can attenuate inflammation and reduce tumor cell proliferation (38). However, in response to DDR, the present study demonstrated the inhibition of Stat3 and NF- κ B following CDCA5 knockdown; this was in contrast to the activation of STAT1/2 and NF- κ B through the cGAS-STING pathway (39). Thus, further investigations are warranted to fully elucidate the underlying mechanisms of CDCA5 knockdown.

Collectively, in response to DNA damage following the knockdown CDCA5, sequential cellular processes occurred, including DDR, cell cycle arrest and the promotion of cell apoptosis. Bcl-2 functions in blocking apoptosis (40). PARP

regulates several biological functions, mainly in the cell survival and cell-death programs (41). PARP is predominantly activated in DDR to cleave PARP and activate target downstream regulators, such as p53 (42). Of note, in the present study, following the knockdown of CDCA5, the decreased expression of transcription factors, such as NF- κ B and Stat3 suggested the inhibition of inflammation. As DDR was induced by the knockdown of CDCA5, CDCA5 may thus be a potential target which may be used in combination with immunotherapy for cancer treatment in the future. As neo-antigens are generated by damaged DNA accumulations, this could increase immunogenicity by stimulating the T-cell response and rendering tumors more susceptible to immunotherapies (43). However, further studies are required to reveal the functions CDCA5 in immune modulation.

In conclusion, the present study demonstrated that CDCA5 overexpression in ccRCC was associated with an advanced TNM stage and pathological grade. The increased expression of CDCA5 predicted a poor survival outcome, whereas its knockdown attenuated cell proliferation and malignancies *in vitro* and *in vivo*. CDCA5 may thus serve as a credible biomarker for the pathological stratification and prognosis of patients, and may prove to be a prospective therapeutic target in the treatment of ccRCC.

Acknowledgements

The authors would like to thank Professor Xue-Min Zhang (State Key Laboratory of Proteomics, National Center of Biomedical Analysis, Beijing, China) for providing technical support.

Funding

The present study was funded by the National Natural Science Foundation of China (NSFC; grant nos. 81972389 and 81770790).

Availability of data and materials

The datasets used and/or analyzed during the current study are available from the corresponding author on reasonable request.

Authors' contributions

XH, YH and XZ conceptualized the study and designed the experiments. XH and ZL performed the experiments, and analyzed and visualized the data. TW, HW and HF assisted with the flow cytometry, animal experiments and processing of images. HF followed-up patients after nephrectomy and generated the tables. SD, SW and DS collected the clinical data. HW and CW were in charge of data mining and curation. XH and YH prepared the manuscript. HL, BW and XZ reviewed and revised the manuscript. XZ, XM, BW and HL provided clinical insight, secured funding and supervised the research. All authors have read and approved the final manuscript for publication. XH, YH, ZL, XM and XZ confirm the authenticity of all the raw data.

Ethics approval and consent to participate

The present study was performed on human cell lines, on animals and retrospectively on formaldehyde-fixed paraffin-embedded tissues from patients. Written informed consent was obtained from all patients. The study was approved by the Protection of Human Subjects Committee of Chinese People's Liberation Army General Hospital (Beijing, China) (S2019-219-07). The scientific use of orthotopic animal models was approved (approval no. ACU20-245) by the Institutional Animal Care and Use Committee (IACUC) of Cyagen Biosciences (Jiangsu, China). The study was performed under the supervision and inspection of the committee and the Cyagen Research Centre for model organisms.

Patient consent for publication

Not applicable.

Competing interests

The authors declare that they have no competing interests.

References

- Bray F, Ferlay J, Soerjomataram I, Siegel RL, Torre LA and Jemal A: Global cancer statistics 2018: GLOBOCAN estimates of incidence and mortality worldwide for 36 cancers in 185 countries. *CA Cancer J Clin* 68: 394-424, 2018.
- Ricketts CJ, De Cubas AA, Fan H, Smith CC, Lang M, Reznik E, Bowlby R, Gibb EA, Akbani R, Beroukhi R, *et al*: The cancer genome atlas comprehensive molecular characterization of renal cell carcinoma. *Cell Rep* 23: 313-326.e5, 2018.
- Cancer Genome Atlas Research Network: Comprehensive molecular characterization of clear cell renal cell carcinoma. *Nature* 499: 43-49, 2013.
- Vasan N, Baselga J and Hyman DM: A view on drug resistance in cancer. *Nature* 575: 299-309, 2019.
- Peters JM: The anaphase promoting complex/cyclosome: A machine designed to destroy. *Nat Rev Mol Cell Biol* 7: 644-656, 2006.
- Rankin S, Ayad NG and Kirschner MW: Sororin, a substrate of the anaphase-promoting complex, is required for sister chromatid cohesion in vertebrates. *Mol Cell* 18: 185-200, 2005.
- Haarhuis JHI, Elbatsh AMO and Rowland BD: Cohesin and its regulation: On the logic of X-shaped chromosomes. *Dev Cell* 31: 7-18, 2014.
- Ladurner R, Kreidl E, Ivanov MP, Ekker H, Idarraga-Amado MH, Busslinger GA, Wutz G, Cisneros DA and Peters JM: Sororin actively maintains sister chromatid cohesion. *EMBO J* 35: 635-653, 2016.
- Sjögren C and Nasmyth K: Sister chromatid cohesion is required for postreplicative double-strand break repair in *Saccharomyces cerevisiae*. *Curr Biol* 11: 991-995, 2001.
- Watrén E and Peters JM: The cohesin complex is required for the DNA damage-induced G2/M checkpoint in mammalian cells. *EMBO J* 28: 2625-2635, 2009.
- Gruber S, Haering CH and Nasmyth K: Chromosomal cohesin forms a ring. *Cell* 112: 765-777, 2003.
- Zhang N and Pati D: Sororin is a master regulator of sister chromatid cohesion and separation. *Cell Cycle* 11: 2073-2083, 2012.
- Tian Y, Wu J, Chagas C, Du Y, Lyu H, He Y, Qi S, Peng Y and Hu J: CDCA5 overexpression is an Indicator of poor prognosis in patients with hepatocellular carcinoma (HCC). *BMC Cancer* 18: 1187, 2018.
- Shen A, Liu L, Chen H, Qi F, Huang Y, Lin J, Sferra TJ, Sankararaman S, Wei L, Chu J, *et al*: Cell division cycle associated 5 promotes colorectal cancer progression by activating the ERK signaling pathway. *Oncogenesis* 8: 19, 2019.
- Chang IW, Lin VCH, He HL, Hsu CT, Li CC, Wu WJ, Huang CN, Wu TF and Li CF: CDCA5 overexpression is an indicator of poor prognosis in patients with urothelial carcinomas of the upper urinary tract and urinary bladder. *Am J Transl Res* 7: 710-722, 2015.
- Fu G, Xu Z, Chen X, Pan H, Wang Y and Jin B: CDCA5 functions as a tumor promoter in bladder cancer by dysregulating mitochondria-mediated apoptosis, cell cycle regulation and PI3k/AKT/mTOR pathway activation. *J Cancer* 11: 2408-2420, 2020.
- Paner GP, Stadler WM, Hansel DE, Montironi R, Lin DW and Amin MB: Updates in the eighth edition of the tumor-node-metastasis staging classification for urologic cancers. *Eur Urol* 73: 560-569, 2018.
- Livak KJ and Schmittgen TD: Analysis of relative gene expression data using real-time quantitative PCR and the 2(-Delta Delta C(T)) method. *Methods* 25: 402-408, 2001.
- Saremi N and Lam AK: Application of tissue microarray in esophageal adenocarcinoma. *Methods Mol Biol* 1756: 105-118, 2018.
- Faustino-Rocha A, Oliveira PA, Pinho-Oliveira J, Teixeira-Guedes C, Soares-Maia R, da Costa RG, Colaço B, Pires MJ, Colaço J, Ferreira R and Ginja M: Estimation of rat mammary tumor volume using caliper and ultrasonography measurements. *Lab Anim (NY)* 42: 217-224, 2013.
- Ma N, Kawanishi M, Hiraku Y, Murata M, Huang GW, Huang Y, Luo DZ, Mo WG, Fukui Y and Kawanishi S: Reactive nitrogen species-dependent DNA damage in EBV-associated nasopharyngeal carcinoma: The relation to STAT3 activation and EGFR expression. *Int J Cancer* 122: 2517-2525, 2008.
- Hanahan D: Hallmarks of cancer: New dimensions. *Cancer Discov* 12: 31-46, 2022.
- Ui A, Chiba N and Yasui A: Relationship among DNA double-strand break (DSB), DSB repair, and transcription prevents genome instability and cancer. *Cancer Sci* 111: 1443-1451, 2020.
- Waldman T: Emerging themes in cohesin cancer biology. *Nat Rev Cancer* 20: 504-515, 2020.
- Xu J, Zhu C, Yu Y, Wu W, Cao J, Li Z, Dai J, Wang C, Tang Y, Zhu Q, *et al*: Systematic cancer-testis gene expression analysis identified CDCA5 as a potential therapeutic target in esophageal squamous cell carcinoma. *EBioMedicine* 46: 54-65, 2019.
- Chen H, Chen J, Zhao L, Song W, Xuan Z, Chen J, Li Z, Song G, Hong L, Song P and Zheng S: CDCA5, Transcribed by E2F1, promotes oncogenesis by enhancing cell proliferation and inhibiting apoptosis via the AKT pathway in hepatocellular carcinoma. *J Cancer* 10: 1846-1854, 2019.
- Nguyen MH, Koinuma J, Ueda K, Ito T, Tsuchiya E, Nakamura Y and Daigo Y: Phosphorylation and activation of cell division cycle associated 5 by mitogen-activated protein kinase play a crucial role in human lung carcinogenesis. *Cancer Res* 70: 5337-5347, 2010.
- Nowak SJ and Corces VG: Phosphorylation of histone H3: A balancing act between chromosome condensation and transcriptional activation. *Trends Genet* 20: 214-220, 2004.
- Lord CJ and Ashworth A: PARP inhibitors: Synthetic lethality in the clinic. *Science* 355: 1152-1158, 2017.
- Mittal P and Roberts CWM: The SWI/SNF complex in cancer-biology, biomarkers and therapy. *Nat Rev Clin Oncol* 17: 435-448, 2020.
- Nishiyama T, Ladurner R, Schmitz J, Kreidl E, Schleiffer A, Bhaskara V, Bando M, Shirahige K, Hyman AA, Mechtler K and Peters JM: Sororin mediates sister chromatid cohesion by antagonizing Wapl. *Cell* 143: 737-749, 2010.
- Losada A: Cohesin in cancer: Chromosome segregation and beyond. *Nat Rev Cancer* 14: 389-393, 2014.
- Bednarski JJ and Sleckman BP: At the intersection of DNA damage and immune responses. *Nat Rev Immunol* 19: 231-242, 2019.
- Chen Q, Sun L and Chen ZJ: Regulation and function of the cGAS-STING pathway of cytosolic DNA sensing. *Nat Immunol* 17: 1142-1149, 2016.
- Cai X, Chiu YH and Chen ZJ: The cGAS-cGAMP-STING pathway of cytosolic DNA sensing and signaling. *Mol Cell* 54: 289-296, 2014.
- Ishikawa H, Ma Z and Barber GN: STING regulates intracellular DNA-mediated, type I interferon-dependent innate immunity. *Nature* 461: 788-792, 2009.

37. Schoggins JW, Wilson SJ, Panis M, Murphy MY, Jones CT, Bieniasz P and Rice CM: A diverse range of gene products are effectors of the type I interferon antiviral response. *Nature* 472: 481-485, 2011.
38. Wang J, Lv X, Guo X, Dong Y, Peng P, Huang F, Wang P, Zhang H, Zhou J, Wang Y, *et al*: Feedback activation of STAT3 limits the response to PI3K/AKT/mTOR inhibitors in PTEN-deficient cancer cells. *Oncogenesis* 10: 8, 2021.
39. Reisländer T, Groelly FJ and Tarsounas M: DNA damage and cancer immunotherapy: A STING in the Tale. *Mol Cell* 80: 21-28, 2020.
40. Danial NN and Korsmeyer SJ: Cell death: Critical control points. *Cell* 116: 205-219, 2004.
41. Schreiber V, Dantzer F, Ame JC and de Murcia G: Poly(ADP-ribose): Novel functions for an old molecule. *Nat Rev Mol Cell Biol* 7: 517-528, 2006.
42. Malanga M and Althaus FR: The role of poly(ADP-ribose) in the DNA damage signaling network. *Biochem Cell Biol* 83: 354-364, 2005.
43. Schumacher TN and Schreiber RD: Neoantigens in cancer immunotherapy. *Science* 348: 69-74, 2015.



This work is licensed under a Creative Commons Attribution-NonCommercial-NoDerivatives 4.0 International (CC BY-NC-ND 4.0) License.